ORIGINAL RESEARCH PAPER

Volume-7 | Issue-7 | July-2018 | PRINT ISSN No 2277 - 8179

INTERNATIONAL JOURNAL OF SCIENTIFIC RESEARCH

NEW METHODS OF IMPLANTED RADIOACTIVE SEEDS ON ULTRASOUND IMAGES USING SUSHISEN ALGORITHM TRUS

Medical Science

Prof P.Senthil Tamilnadu open university &Tiruchirappalli

Prof M.Suganya* Tamilnadu open university &Tiruchirappalli *Corresponding Author

ABSTRACT

A common modality for the treatment of early stage prostate cancer is the implantation of radioactive seeds directly into the prostate. The radioactive seeds are positioned inside the prostate to achieve optimal radiation dose coverage to the prostate. These radioactive seeds are positioned inside the prostate using TRUS imaging. Once all of the planned seeds have been implanted, two dimensional images separated by 2 mm are obtained throughout the prostate, beginning at the base of the prostate up to and including the apex. A common deep neural network, called Bounding box was trained to automatically determine the position of the implanted radioactive seeds within the prostate under ultrasound imaging. The results of the training using 1950 training ultrasound images and 90 validation ultrasound images. The commonly used metrics for successful training were used to evaluate the efficacy and accuracy of the trained deep neural network and resulted in an loss_bbox (train) = 0.00, loss_coverage (train) = 2.99e-8, loss_bbox (validation) = 12.84, loss_coverage (validation) = 9.70, mAP (validation) = 66.87%, precision (validation) = 84.07%, and a recall (validation) = 87.29%, where train and validation refers to the training image set and validation refers to the validation training set. On the hardware platform used, the training expended 11.8 seconds per epoch. The network was trained for over 10,000 epochs. In addition the seed locations as determined by the Deep Neural Network were compared to the seed locations as determined sushisen algorithms based on a one to three months after implant CT. The Deep Learning approach was within 2.29 mm of the seed locations determined research analysis. The Deep Learning approach to the determination of radioactive seed locations is robust, accurate, and fast and well within spatial agreement with the gold standard of CT determined seed coordinates.

KEYWORDS

Deep Neural Network ,trus , Bounding Box ,sushisen Algorithms

INTRODUCTION

The treatment of early stage prostate cancer using the implantation of radioactive seeds has a long and successful history [1-4]. The typical procedure begins with the acquisition of ultrasound images of the prostate. Once obtained, computer software is used to determine the optimal placement of the seeds within the prostate. Isotopes that are commonly used for prostate seed implantation are I^{125},Pd^{103},and Au^{198} . The seeds are implanted transperineally into the prostate using 18 gauge needles that are loaded according to the optimal seed locations as determined by the commercial software. Needles are guided into the prostate using a rectangular grid of guide holes. There are 14 guide holes across and 14 guide holes down all equally spaced at 2.5 mm. The needles can be loaded with radioactive seeds as well as plastic spacers. The spacers are the same length as the seeds, which is approximately 0.5 cm. Therefore the planned spatial coordinates of the implanted seeds are discrete. If a coordinate system is chosen such that the x-coordinate goes left to right, the y-coordinate up and down and the z-coordinate into the prostate, the only available seed coordinates are ($i \cdot dx, j \cdot dy, k \cdot dz$) where dx=dy=0.25 cm and dz=0.2 cm and i,j,k are integers.

Once an optimal plan is generated, termed the pre-plan, the seeds are implanted into the prostate according to this treatment plan. This procedure in which the pre-plan is done with in the operating room is termed intra-operative pre-planning. Due to variations in tissue density, elasticity, and operator expertise, the seeds are not deposited exactly as intended. Holupka et. al. has measured this variation and the actual deposited position of the seeds differs on average from the intended position of the seeds by approximately 2 mm [5].

In the current procedure, the patient is released after the implantation and returns for a follow up CT scan approximately six weeks later. A transaxial CT scan of the prostate is obtained at 2 mm image separation. The spatial position of the implanted seeds are then automatically determined using a number of commercially available software applications. In this study Variseed (Varian Medical Solutions, Palo Alto CA) was used. The radiation dose distribution is then determined based on the seed positions as determined by Variseed. This radiation plan can then be evaluated in terms of its compliance to the physicians clinical objective. The clinical objective is defined as the physician's required radiation dose coverage of the Planned Target Volume (PTV) as well as radiation dose constraints on healthy tissue structures such as the urethra, rectum and bladder. This radiation plan is termed the "post-plan".

It would be ideal if the post-plan could be performed in the operating room immediately after the implantation. The physician can inform the patient immediately how well the procedure went as well as add additional seeds if a particular area of the prostate received less than the intended dose. Since ultrasound is the modality of choice in the operating room, an automatic post-plan must be based on ultrasound not CT. While many attempts have been made to create an ultrasound based post-planning application, either they have failed or have limited success. This failure is in part due to the difficulty in identifying seeds on ultrasound. Even the "expert" defined seed locations used in this study can arguably be called somewhat accurate at best. In all reality the neural network may in fact be more accurate than the human defined seed positions, which puts the ground truth somewhat in doubt. However, suffice it to say that the real measure of the inferred seed positions as determined by the neural network has to be compared to the "gold standard" of the CT based seed positions. The true accuracy of the neural network's ability to accurately determine seed positions on ultrasound will be measured in this study.

PURPOSE

GPUs tend to have many thousand more computational cores than a conventional CPU and have the ability to rapidly teach these deep neural networks to "learn" such things as image recognition, object detection and segmentation on medical images. These platforms are a combination of MATLAB 2017B programs that have been vetted and perform quite well. All of these routines are made transparent by the use of Bounding box in DIGITS, made popular by NVIDIA, which is an MATLAB 2017B based wrapper around these routines. Bounding box makes accessible the use of Deep Learning to the average medical researcher yielding fast and accurate results. NVIDIA currently supplies a range of GPU based graphics cards that can be used in Deep Learning.

CT imaging is currently the gold standard for the determination of radioactive seed locations within the prostate for post intra operative implantation. However, CT imaging is expensive and not readily available in the operating room. The ability to detect the spatial location of radioactive seeds implanted inside the prostate on ultrasound imaging has been a long standing problem. The solution should be fast, obtained within a few seconds or minutes, and accurate relative to the spatial location of the seeds as determined by CT imaging.

ALGORITHM:SUSHISEN

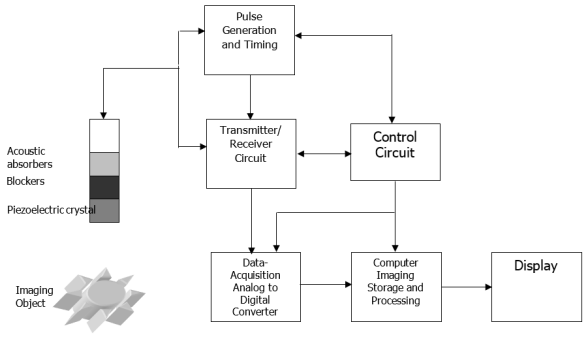

Input: A List TRUS Of Numbers L.
Output: The Largest CT Number In The List L.

1. int = *I*ntensity in $dB = 10\log_{10}\frac{I_1}{I_2} =$

$R_0 = I_0(1-R_{12}^2)(1-R_{23}^2)(1-R_{34}^2)R_{45}$

2. If L.Size = 0 Return Null

$$J_{cr}(t) = K\left|\iiint_{\Re} R(x,y,z)s(x,y)\overline{\omega}\left(t-\frac{2z}{c}\right)dxdydz\right|$$

3. Largest ← L[0];
4. For Each Item In L, Do
5. If Item > Largest, Then;
6. Largest ← Item;
7. Return Largest;
8. Print "Type Trus Greater Than 0";

9. Input A,B= ($R_0 = I_0T_{12}T_{23}T_{34}T_{54}T_{43}T_{32}T_{21}$)

10. If B=0 Then Goto 80;
11. If A > B Then Goto 60;
12. Let A =

$$J_{cr}(t) = K\left|R\left(x,y,\frac{ct}{2}\right)\otimes s(-x,-y)\overline{\omega}(t)\right|$$

13. Goto 20;
14. Let A=A-B;
15. Goto 20;
16. Print A=

$$J_r(t) = K\left|\iiint_{\Re}\left(\frac{e^{-2\mu z}}{z}\right)R(x,y,z)s(x,y)\overline{\omega}\left(t-\frac{2z}{c}\right)dxdydz\right|$$

17. End;

Assume an image $I\mu\ 1 \le \mu \le N_{images} I\mu$

where $N_{imagesis}$ the total number of images, $N_{images} = N_{training}$+N validation, where $N_{training}$ are the number of training images and N validation is the number of validation images. Let every image be covered by a uniform rectangular grid where each grid rectangle is uniformly $N_{grid}\ xM_{grid}$ pixels.

For convenience define

$N_{TBBI}\ \mu) \equiv$ *True Number Bounding Boxes Per Image* μ ,(1)
$N_{PBBI}\mu) \equiv$ *redicted Number Bounding Boxes Per Image* (2)
$N_{G\mu} \equiv$ *Number of Grid Rectangles Per Image* μ (3)

Therefore the coverage of a true bounding box of area, $A_{i\mu}$, $1 \le_{i\mu} \le N_{TBBI\mu}$) , $1 \le \mu \le N_{images}$ by a grid square $gj\mu$, $1 \le j\mu \le N_{G\mu}$ is

$$coverage\left(A_{i_\mu}\right) = \sum_{j_\mu=1}^{N_{G_\mu}} \frac{Area(A_{i_\mu} \cap g_{j_\mu})}{Area(g_{j_\mu})} \in [0,1] \text{ ,(4)} \quad \text{,(5)}$$

$$IOU_{A_{i_\mu}B_{j_\mu}} = \frac{Area(A_{i_\mu} \cap B_{j_\mu})}{Area\left(A_{i_\mu}\right)+Area\left(B_{j_\mu}\right)-Area(A_{i_\mu} \cap B_{j_\mu})} > \lambda \text{ ,}$$
(6)

where λ is some threshold then $B_{i\mu}$ is a true positive else it is not a true positive (either true negative or false positive).

The precision and recall for the validation set is defined

$$Precision_{validation} = \sum_{\mu=1}^{N_{validation}} \frac{N_{True\ Positives_\mu}}{N_{True\ Positives_\mu}+N_{False\ Positives_\mu}} \in [0,1] \text{ .}$$
(7)

$$Recall_{validation} = \sum_{\mu=1}^{N_{validation}} \frac{N_{True\ Positives_\mu}}{N_{True\ Positives_\mu}+N_{False\ Negatives_\mu}} \in [0,1] \text{ ,}$$
(8)

where $N_{\text{True Positives }\mu}$ is defined as the number of true positives on image μ , $N_{False\ Positives\ \mu}$ is defined as the number of false positives on image μ and $N_{FalseNegatives\mu}$ is the number of false negatives on image μ.

The *coverageloss* is defined as the *coverage(A)−coverage(B)*. The *mAP* is the product of the *precision* and the *recall*, specifically

$$maP = \sum_{\mu=1}^{N_{validation}} \left(\frac{N_{True\ Positives_\mu}}{N_{True\ Positives_\mu}+N_{False\ Positives_\mu}}\right) \cdot \left(\frac{N_{True\ Positives_\mu}}{N_{True\ Positives_\mu}+N_{False\ Negatives_\mu}}\right) \text{ ,}$$
(9)

bbox_loss is defined as the differences in the left lower corner of the true bounding box and the predicted right upper corner and left lower corner of the predicted bounding box.

Therefore the performance of Bounding box is based on the values of loss_bbox (training), loss_bbox(validation), loss_coverage (valuation), mAP (valuation), precision (valuation) recall (valuation) and, loss_coverage (training). The deep neural network adapts the weights per node so as to minimize the valuation loss coverage and the weights are adjusted accordingly. The weights are adjusted according to the gradient descent method used here (ADAM).

Results

Training Bounding box on the radioactive seed implanted ultrasound images consisted of 1517 training images, and 231 validation images. The hardware platform used was a Whisper Station consisting of four Intel Xeon E5-1600v4 CPUs, NVIDIA Quadro K420, 4 NVIDIA GeForce GTX Titan-X GPUs. CUDA and DIGITS came pre-installed using the Ubuntu 16.04 operating system. It took approximately 12.8 seconds per epoch at the current training and validation image set size.

Figure 2 displays a typical learning curve for Bounding box where the loss drops initially and the mAP raises above zero. Bounding box was successfully trained to determine the location of implanted radioactive seeds on ultrasound imaging. Figure 1 also shows some typical inferences from the validation image set. It is noticed that even with a modest mAP value of 66.87% the inferences of where the seeds are located on the validation images is quite exact. The trained Bounding box inference takes approximately 0.2052 seconds per ultrasound image.

Comparison to CT Images: The seed locations of ten patients of the training set images as well as the validation set images were compared to the seed locations as determined by the commercial software called Variseed by Varian Medical Systems, Palo Alto, Ca. Variseed uses a robust algorithm to determine the seed locations on the CT images obtained for each of the patients in this study. These seed locations can be exported as text files and are easily compared to the inferred seed locations determined by trained Bounding box. Since it is not uncommon for the CT images to be obtained one to three months or so after the implant (while the ultrasound images presented to Bounding box are obtained on the day of the implant procedure) the seed locations may be different by a scale factor since adema may have set in during the procedure. This scale factor is represented asymmetricallyComparison to CT Images: The seed locations of ten

patients of the training set images as well as the validation set images were compared to the seed locations as determined by the commercial software called Variseed by Varian Medical Systems, Palo Alto, Ca. Variseed uses a robust algorithm to determine the seed locations on the CT images obtained for each of the patients in this study. These seed locations can be exported as text files and are easily compared to the inferred seed locations determined by trained Bounding box. Since it is not uncommon for the CT images to be obtained one to three months or so after the implant (while the ultrasound images presented to Bounding box are obtained on the day of the implant procedure) the seed locations may be different by a scale factor since adema may have set in during the procedure. This scale factor is represented asymmetrically as $(s_x,s_y,s_z) \in \mathbb{R}^3$ and represents by how much the prostate gland has spatially changed its shape. In addition the seed locations as determined by Bounding box may be different both translationally and rotationally from that of the CT coordinates. To bring the inferred seed coordinates as determined by Bounding box to be in the same spatial coordinate system as used by Variseed and to determine the minimal distance these seeds can be, a program was developed in the *MATLAB2017B* programming language, that rotates, translates, and scales the inferred ultrasound seed coordinates, or the coordinates of the seeds as determined by Bounding box, so the minimal distance between the CT coordinates and the ultrasound coordinates are at a minimum. First the program determines the center of mass of all seed artifacts in the ten patients studied and brings both the CT defined seed coordinates to its center of mass as well as the inferred, by Bounding box, ultrasound seed coordinates to their center of mass. This program loops over all rotations and scales in the range of Sushisen algorithms.

TABLE I:TRUS

Sample size =DS	50
Prevalence =μ	0.660
Sensitivity =α	0.758
Specificity =ƨ	0.941
PPV =ρ	0.962
NPV =	0.667
LR + result*=	12.879
LR - result*=	0.258

$$R_{x,y,z} \in [-10^0, 10^0] \; and \; S_{x,y,z} \in [0.70, 1.30] \quad (10)$$

where $R_{x,y,z}$ is the angular rotation in degrees (ultimately represented as the Euler matrix) in the *x,y*, or z directions, and $S_{x,y,z}$ is the anisotropic scaling factor (representing adema) in the *x,y*, or *z* directions. These transformations are determined for all Bounding box inferred ultrasound seed coordinates as compared to each single, individual seed coordinate of the CT set. The minimal distance obtained, as well as the transformation that determined this minimal distance is reported by the program. While this represents the best of all possible worlds, it is the best minimal distance these seeds can be located relative to each other. The program loops over all possible transformations as determined by the intervals of equation 10.

The results over all seed locations for the seed locations determined by inference of the best Bounding box metric values for the validation set as compared to the CT coordinates as determined by the Variseed software were determined to be within on average 2.29 mm of each other. This reported value is a few millimeters and represents excellent agreement between the trained Bounding box inferred seed locations and the CT based seed locations.

Discussion

An artificial deep convolution neural network was trained on thousands of ultrasound images containing implanted seed artifacts. The seeds were trained by an expert (one of the authors) to indicate where the radioactive seeds were located on each image. Approximately 15% of these ultrasound images were used as an example set, termed the validation set, of which the deep convolution network never saw before, and the seeds were inferred on this set as well. The inferred seed locations were compared to the gold standard laid down by the industry of the CT seed coordinates and the inferred seed locations were in fact very close to the CT seed coordinates. 10 patients were studied in this manner and the inferred seed locations compared to the CT seed locations were 2.29 mm of each other.

Conclusion

An automated method to detect the spatial positions of radioactive seeds implanted into the human prostate was developed by training the Deep Neural network Bounding box. loss_bbox (train) = 0.00, loss_coverage (train) = 1.89e-8, loss_bbox (validation) = 11.84, loss_coverage (validation) = 9.70, mAP (validation) = 66.87%, precision (validation) = 81.07%, and a recall (validation) = 82.29%, where train and validation refers to the training image set and validation refers to the validation training set. The network was trained for over 10,000 epochs. The trained Bounding box inference takes approximately 0.2052 seconds per ultrasound image. There are typically 8-12 intraoperative ultrasound images taken. This results in approximately 2.052 seconds per patient study.

Bounding box performed very well for the problem of automatically detecting the spatial position on ultrasound imaging of radioactive seeds implanted in the prostate. Future plans for the clinical implementation of Bounding box will be to detect the radioactive seeds and then perform an accurate dose calculation to evaluate the efficacy of the therapy in the operating room.

The agreement with the seed coordinates as determined by the commercial software, Variseed, and the inference seed positions from the CNN was determined to be with 2.29 mm of each other. This type of agreement is excellent for automatic determination of seed locations using either imaging modality, ultrasound or CT[5].

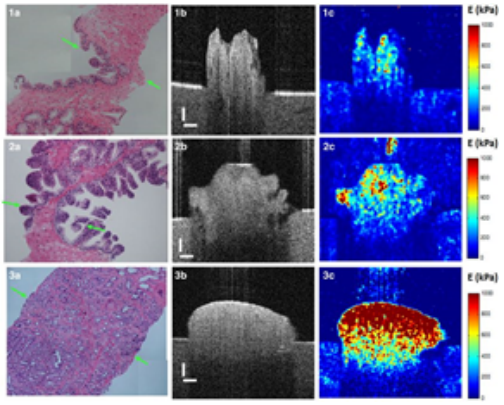

Figure 1: (a) Sample ultrasound images of the prostate, (b,c) inference of where the predicted seeds are on validation images.

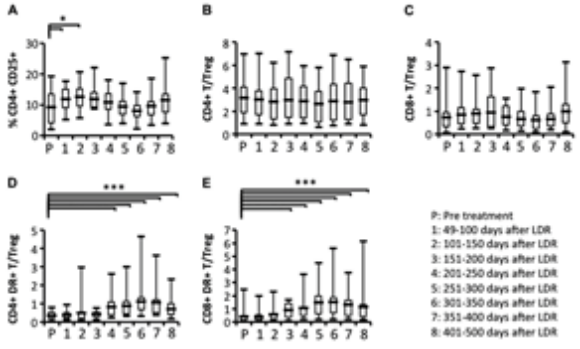

Figure 2: Typical learning curves associated with the training of Bounding box for the purpose of identifying radiation seeds implanted into the prostate.

ACKNOWLEDGEMENTS

This paper is made possible through the help and support from everyone, father N.Periyasamy and Chinnaponnu mother Daughter S.S.Inakshi in varagubady or varagupadi village and in essence, all sentient beings. I sincerely thank to my parents, family, and friends, who provide the advice and financial support. The product of this paper would not be possible without all of them.

References

1. Esteva A, Kuprel B, Novoa RA, Ko J, Swetter SM, Blau HM, Thrun S., "Dermatologist-level classification of skin cancer with deep neural networks.", Nature. 542, 15-18 (2017).
2. Kumar A, Kim J, Lyndon D, Fulham M, Feng D., "An Ensemble of Fine-Tuned Convolutional Neural Networks for Medical Image Classification.", IEEE J Biomed Health Inform. 21(1), 31-40 2016.
3. Tajbakhsh N, Shin JY, Gurudu SR, Hurst RT, Kendall CB, Gotway MB, Liang J., "Convolutional Neural Networks for Medical Image Analysis: Fine Tuning or Full

Training?", IEEE Trans Med Imaging. 35(5), 1299-1312 (2016).
4. Bittner NH, Orio PF 3rd, Merrick GS, Prestidge BR, Hartford AC, Rosenthal , "The American College of Radiology and the American Brachytherapy Society practice parameter for transperineal permanent brachytherapy of prostate cancer.", Bracytherapy 16(1), 59-67 (2017).
5. Davis BJ, Taira AV, Nguyen PL, Assimos DG, D'Amico AV, Gottschalk AR, Gustafson GS, Keole SR, Liauw SL, Lloyd S, McLaughlin PW, Movsas B, Prestidge BR, Showalter TN, Vapiwala N., "ACR appropriateness criteria permanent source brachytherapy for prostate cancer.", Brachytherapy 16(2), 266-276 (2017).
6. Bues M1, Holupka EJ, Meskell P, Kaplan ID, "Effect of random seed placement error in permanent transperineal prostate seed implant", RadiotherOncol. 79(1), 70-74 (2006).
7. Shi J, Liu Q, Wang C, Zhang Q, Ying S, Xu H., "Super-resolution reconstruction of MR image with a novel residual learning network algorithm.", Phys Med. Biol. Accepted Mar. 27 (2018)
8. Zhu B, Liu JZ, Cauley SF, Rosen BR, Rosen MS., "Image reconstruction by domain-transform manifold learning.", Nature. 21(555), 487-492 (2018).
9. Rachmadi MF, Valdés-Hernández MDC, Agan MLF, Di Perri C, Komura T, "Alzheimer's Disease Neuroimaging Initiative. Segmentation of white matter hyperintensities using convolutional neural networks with global spatial information in routine clinical brain MRI with none or mild vascular pathology.",Comput. Med. Imaging Graph. 17(66), 28-43 (2018).
10. Antropova N, Abe H, Giger ML., "Use of clinical MRI maximum intensity projections for improved breast lesion classification with deep convolutional neural networks.", J. Med. Imaging (Bellingham) 5(1), 1-10 (2018)
11. Nie D, Wang L, Trullo R, Li J, Yuan P, Xia J, Shen D., "Segmentation of Craniomaxillofacial Bony Structures from MRI with a 3D Deep-Learning Based Cascade Framework.". Mach. Learn. Med. Imaging. 10541(1), 266-273 (2017).
12. Alex V, Vaidhya K, Thirunavukkarasu S, Kesavadas C, Krishnamurthi G., "Semisupervised learning using denoisingautoencoders for brain lesion detection and segmentation.", Jour. Med. Imaging . 4(4), 1-11 (2017).
13. Han L, Kamdar MR., "MRI to MGMT: predicting methylation status in glioblastoma patients using convolutional recurrent neural networks.", Pac. Symp. Biocomput. 23,331-342 (2018).
14. Xiang L, Qiao Y, Nie D, An L, Wang Q, Shen D., "Deep Auto-context Convolutional Neural Networks for Standard-Dose PET Image Estimation from Low-Dose PET/MRI.", Neurocomputing. 267, 406-416 (2017).
15. Wang X, Yang W, Weinreb J, Han J, Li Q, Kong X, Yan Y, Ke Z, Luo B, Liu T, Wang L., "Searching for prostate cancer by fully automated magnetic resonance imaging classification: deep learning versus non-deep learning.", Sci. Rep. 13(7), 1-15 (2017).
16. Liu Y, Stojadinovic S, Hrycushko B, Wardak Z, Lau S, Lu W, Yan Y, Jiang SB, Zhen X, Timmerman R, Nedzi L, Gu X., "A deep convolutional neural network-based automatic delineation strategy for multiple brain metastases stereotactic radiosurgery.", PLoS One. 12(10), 1-15 (2017)
17. Liu F, Jang H, Kijowski R, Bradshaw T, McMillan AB., "Deep Learning MR Imaging-based Attenuation Correction for PET/MR Imaging.", Radiology. 286(2),676-684 (2018).
18. Li Z, Wang Y, Yu J, Guo Y, Cao W. "Deep Learning based Radiomics (DLR) and its usage in noninvasive IDH1 prediction for low grade glioma.", Sci. Rep. 17(1), 1-11 (2017).
19. Trebeschi S, van Griethuysen JJM, Lambregts DMJ, Lahaye MJ, Parmar C, Bakers FCH, Peters NHGM, Beets-Tan RGH, Aerts HJWL., "Deep Learning for Fully-Automated Localization and Segmentation of Rectal Cancer on Multiparametric MR.", Sci. Rep. 7(1), 1-9 (2017)
20. Azizi S, Bayat S, Yan P, Tahmasebi A, Nir G, Kwak JT, Xu S, Wilson S, Iczkowski KA, Lucia MS, Goldenberg L, Salcudean SE, Pinto PA, Wood B, Abolmaesumi P, Mousavi P., "Detection and grading of prostate cancer using temporal enhanced ultrasound: combining deep neural networks and tissue mimicking simulations.", Int. J. Comput. Assist. Radiol. Surg. 12(8),1293-1305 (2017).
21. Le MH, Chen J, Wang L, Wang Z, Liu W, Cheng KT, Yang X., "Automated diagnosis of prostate cancer in multi-parametric MRI based on multimodal convolutional neural networks.", Phys Med Biol. 62(16),6497-6514 (2017).